estimate the drug metabolism capacity, the amount of metabolites must be measured during the time when production of metabolites is linearly detected (generally before 24 h). To the best of our knowledge, there have been few reports that have examined various drugs metabolism capacity of hESC-hepa and hiPSC-hepa in detail.

In the present study, seven candidate genes (*FOXA2*, *HEX*, *HNF1α*, *HNF1β*, *HNF4α*, *HNF6*, and *SOX17*) were transduced into each stage of hepatic differentiation from hESCs by using an adenovirus (Ad) vector to screen for hepatic differentiation-promoting factors. Then, hepatocyte-related gene expression profiles and hepatocyte functions in hESC-hepa and hiPSC-hepa generated by the optimized protocol, were examined to investigate whether these cells have PHs characteristics. We used nine drugs, which are metabolized by various CYP enzymes and UDP-glucuronosyltransferases (UGTs), to determine whether the hESC-hepa and hiPSC-hepa have drug metabolism capacity. Furthermore, hESC-hepa and hiPSC-hepa were examined to determine whether these cells may be applied to evaluate drug-induced cytotoxicity.

Materials and methods

In vitro differentiation

Before the initiation of cellular differentiation, the medium of hESCs and hiPSCs was exchanged for a defined serum-free medium, hESF9, and cultured as previously reported [9]. The differentiation protocol for the induction of DE cells, hepatoblasts, and hepatocytes was based on our previous report with some modifications [5,6]. Briefly, in mesendoderm differentiation, hESCs and hiPSCs were dissociated into single cells by using Accutase (Millipore) and cultured for 2 days on Matrigel (BD biosciences) in differentiation hESF-DIF medium which contains 100 ng/ml Activin A (R&D Systems) and 10 ng/ml bFGF (hESF-DIF medium, Cell Science & Technology Institute; differentiation hESF-DIF medium was supplemented with 10 μg/ml human recombinant insulin, 5 μg/ml human apotransferrin, 10 μM 2-mercaptoethanol, 10 μM ethanolamine, 10 μM sodium selenite, and 0.5 mg/ml bovine serum albumin, all from Sigma). To generate DE cells, mesendoderm cells were transduced with 3000 VP/cell of Ad-FOXA2 for 1.5 h on day 2 and cultured until day 6 on Matrigel in differentiation hESF-DIF medium supplemented with 100 ng/ml Activin A and 10 ng/ml bFGF. For induction of hepatoblasts, the DE cells were transduced with each 1500 VP/cell of Ad-FOXA2 and Ad-HNF1α for 1.5 h on day 6 and cultured for 3 days on Matrigel in hepatocyte culture medium (HCM, Lonza) supplemented with 30 ng/ml bone morphogenetic protein 4 (BMP4, R&D Systems) and 20 ng/ml FGF4 (R&D Systems). In hepatic expansion, the hepatoblasts were transduced with each 1500 VP/cell of Ad-FOXA2 and Ad-HNF1α for 1.5 h on day 9 and cultured for 3 days on Matrigel in HCM supplemented with 10 ng/ml hepatocyte growth factor (HGF), 10 ng/ml FGF1, 10 ng/ml FGF4, and 10 ng/ml FGF10 (all from R&D Systems). In hepatic maturation, cells were cultured for 8 days on Matrigel in L15 medium (Invitrogen) supplemented with 8.3% tryptose phosphate broth (BD biosciences), 10% FBS (Vita), 10 μM hydrocortisone 21-hemisuccinate (Sigma), 1 μM insulin, 25 mM $NaHCO_3$ (Wako), 20 ng/ml HGF, 20 ng/ml Oncostatin M (OsM, R&D systems), and 10^{-6} M Dexamethasone (DEX, Sigma).

Results

Recently, we showed that the sequential transduction of SOX17, HEX, and HNF4α into hESC-derived mesendoderm, DE, and hepatoblasts, respectively, leads to efficient generation of the hESC-hepa [5–7]. In the present study, to further improve the differentiation efficiency towards hepatocytes, we screened for hepatic differentiation-promoting transcription factors. Seven candidate genes involved in liver development were selected. We then examined the function of the hESC-hepa and hiPSC-hepa generated by the optimized protocol for pharmaceutical use in detail.

Efficient hepatic differentiation by Ad-FOXA2 and Ad-HNF1α transduction

To perform efficient DE differentiation, T-positive hESC-derived mesendoderm cells (day 2) (Supplementary Fig. 1) were transduced with Ad vector expressing various transcription factors (Ad-FOXA2, Ad-HEX, Ad-HNF1α, Ad-HNF1β, Ad-HNF4α, Ad-HNF6, and Ad-SOX17 were used in this study). We ascertained the expression of *FOXA2*, *HEX*, *HNF1α*, *HNF1β*, *HNF4α*, *HNF6*, or *SOX17* in Ad-FOXA2-, Ad-HEX-, Ad-HNF1α-, Ad-HNF1β-, Ad-HNF4α-, Ad-HNF6-, or Ad-SOX17-transduced cells, respectively (Supplementary Fig. 2). We also verified that there was no cytotoxicity of the cells transduced with Ad vector until the total amount of Ad vector reached 12,000 VP/cell (Supplementary Fig. 3). Each transcription factor was expressed in hESC-derived mesendoderm cells on day 2 by using Ad vector, and the efficiency of DE differentiation was examined (Fig. 1A). The DE differentiation efficiency based on CXCR4-positive cells was the highest when Ad-SOX17 or Ad-FOXA2 were transduced (Fig. 1B). To investigate the difference between Ad-FOXA2-transduced cells and Ad-SOX17-transduced cells, gene expression levels of markers of undifferentiated cells, mesendoderm cells, DE cells, and extraembryonic endoderm cells were examined (Fig. 1C). The expression levels of extraembryonic endoderm markers of Ad-SOX17-transduced cells were higher than those of Ad-FOXA2-transduced cells. Therefore, we concluded that FOXA2 transduction is suitable for use in selective DE differentiation.

To promote hepatic commitment, various transcription factors were transduced into DE cells and the resulting phenotypes were examined on day 9 (Fig. 1D). Nearly 100% of the population of Ad-FOXA2-transduced cells and Ad-HNF1α-transduced cells was α-fetoprotein (AFP)-positive (Fig. 1E). We expected that hepatic commitment would be further accelerated by combining FOXA2 and HNF1α transduction. The DE cells were transduced with both Ad-FOXA2 and Ad-HNF1α, and then the gene expression levels of *CYP3A7* [10], which is a marker of fetal hepatocytes, were evaluated (Fig. 1F). When both Ad-FOXA2 and Ad-HNF1α were transduced into DE cells, the promotion of hepatic commitment was greater than in Ad-FOXA2-transduced cells or Ad-HNF1α-transduced cells.

To promote hepatic expansion and maturation, we transduced various transcription factors into hepatoblasts on day 9 and 12 and the resulting phenotypes were examined on day 20 (Fig. 1G). We ascertained that the hepatoblast population was efficiently expanded by addition of HGF, FGF1, FGF4, and FGF10 (Supplementary Fig. 4). The hepatic differentiation efficiency based on asialoglycoprotein receptor 1 (ASGR1)-positive cells was measured on day 20, demonstrating that FOXA2, HNF1α, and HNF4α transduction could promote efficient hepatic maturation (Fig. 1H). To investigate the phenotypic difference between Ad-FOXA2-, Ad-HNF1α-, and Ad-HNF4α-transduced cells, gene expression levels of early hepatic markers, mature hepatic markers, and biliary markers were examined (Fig. 1I). Gene expression levels of mature hepatic markers were up-regulated by FOXA2, HNF1α, or HNF4α transduction. FOXA2 transduction strongly upregulated gene expression levels of both early hepatic markers and mature hepatic markers, while HNF1α or HNF4α transduc-

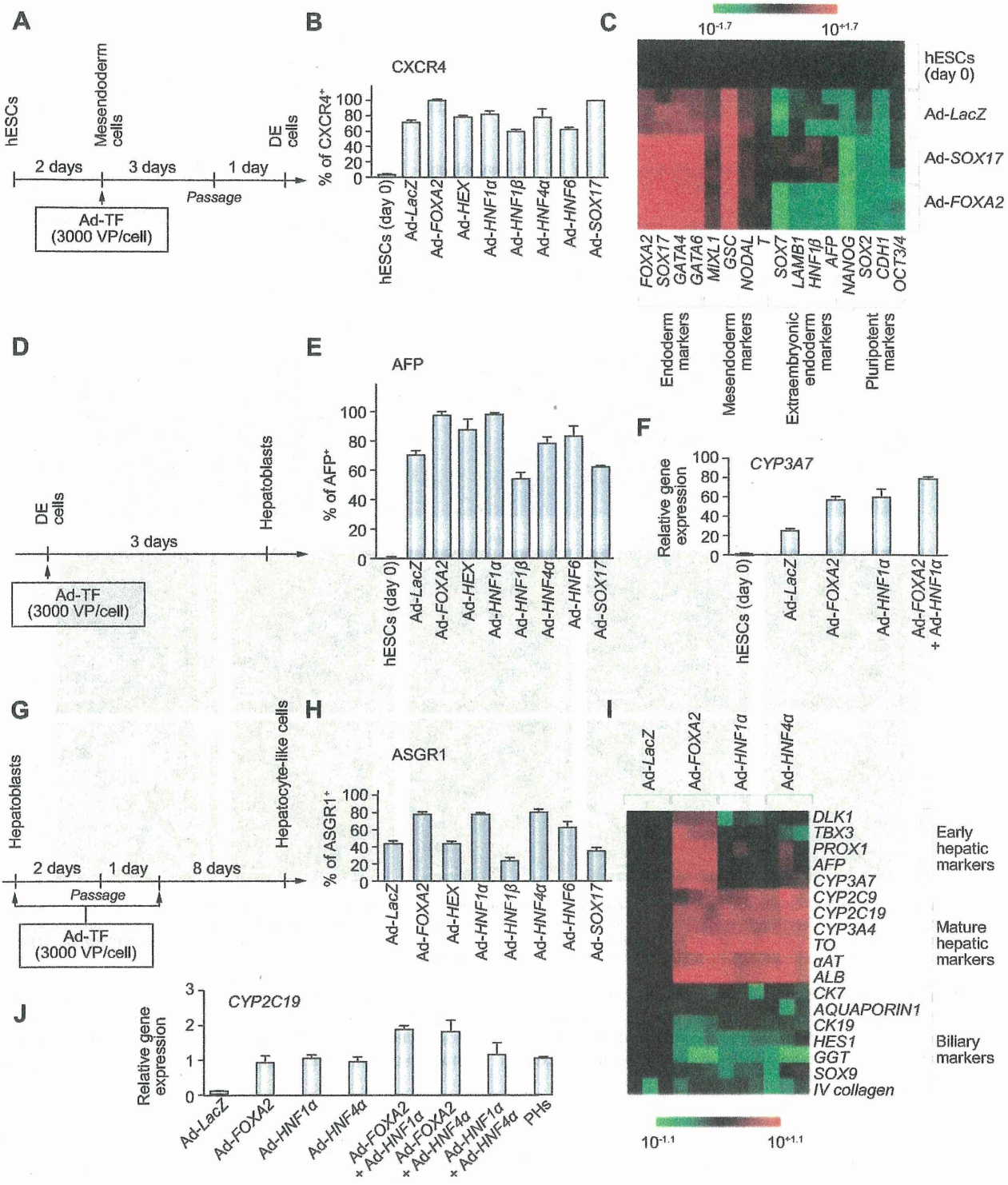

Fig. 1. Efficient hepatic differentiation from hESCs by FOXA2 and HNF1α transduction. (A) The schematic protocol describes the strategy for DE differentiation from hESCs (H9). Mesendoderm cells (day 2) were transduced with 3000 VP/cell of transcription factor (TF)-expressing Ad vector (Ad-TF) for 1.5 h and cultured as described in Fig. 2A. (B) On day 5, the efficiency of DE differentiation was measured by estimating the percentage of CXCR4-positive cells using FACS analysis. (C) The gene expression profiles were examined on day 5. (D) Schematic protocol describing the strategy for hepatoblast differentiation from DE. DE cells (day 6) were transduced with 3000 VP/cell of Ad-TF for 1.5 h and cultured as described in Fig. 2A. (E) On day 9, the efficiency of hepatoblast differentiation was measured by estimating the percentage of AFP-positive

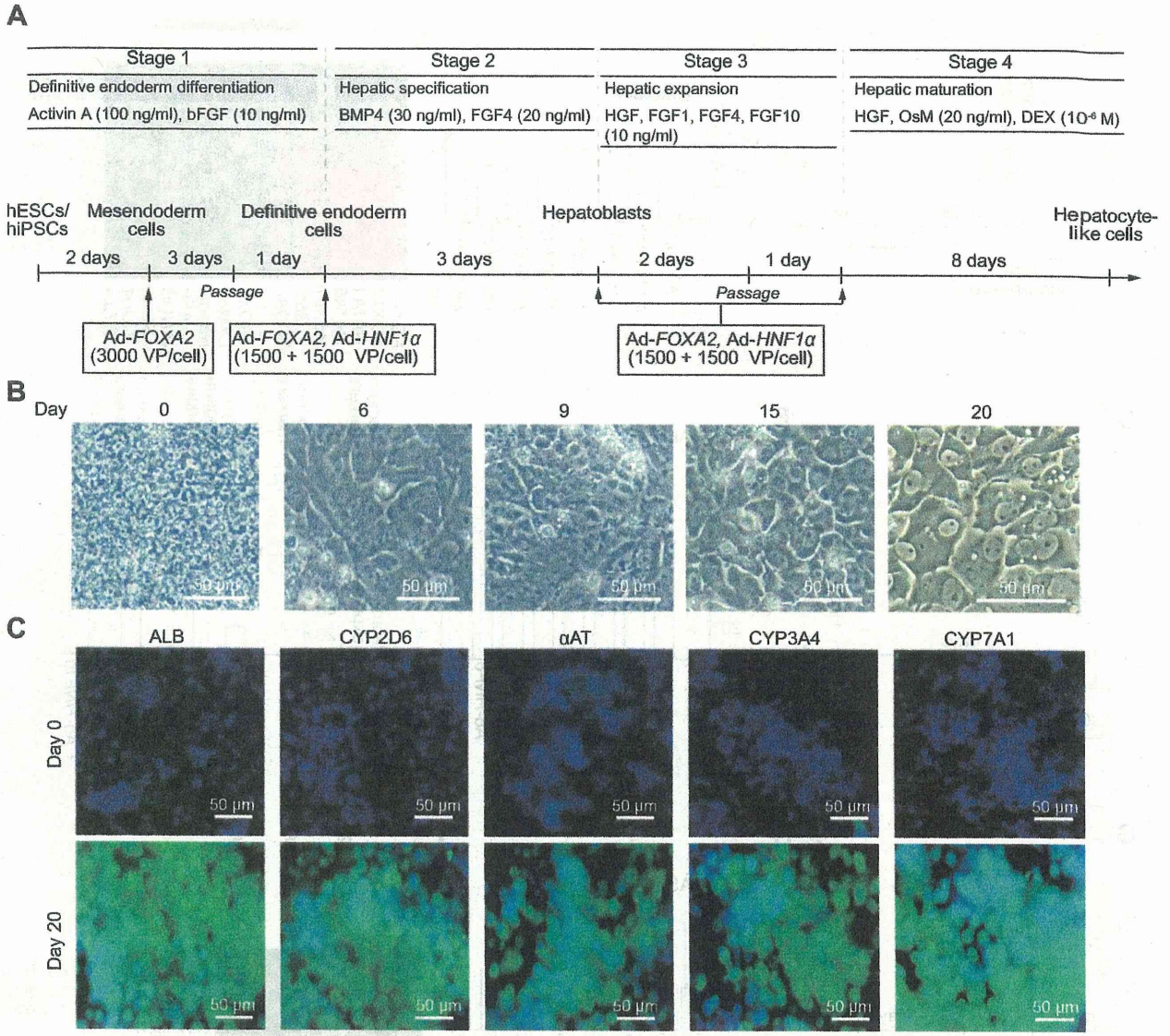

Fig. 2. Hepatic differentiation of hESCs and hiPSCs by FOXA2 and HNF1α transduction. (A) The differentiation procedure of hESCs and hiPSCs into hepatocytes via DE cells and hepatoblasts is schematically shown. Details of the hepatic differentiation procedure are described in Materials and methods. (B) Sequential morphological changes (day 0–20) of hESCs (H9) differentiated into hepatocytes are shown. (C) The expression of the hepatocyte markers (ALB, CYP2D6, αAT, CYP3A4, and CYP7A1, all green) was examined by immunohistochemistry on day 0 and 20. Nuclei were counterstained with DAPI (blue).

tion did not up-regulate the gene expression levels of early hepatic markers. Next, multiple transduction of transcription factors was performed to promote further hepatic maturation. The combination of Ad-FOXA2 and Ad-HNF1α transduction and the combination of Ad-FOXA2 and Ad-HNF4α transduction result in the most efficient hepatic maturation, judged from the gene expression levels of *CYP2C19* (Fig. 1J). This may happen because the mixture of immature hepatocytes and mature hepatocytes coor-

cells using FACS analysis. (F) The gene expression level of *CYP3A7* was measured by real-time RT-PCR on day 9. On the *y* axis, the gene expression level of *CYP3A7* in hESCs (day 0) was taken as 1.0. (G) The schematic protocol describes the strategy for hepatic differentiation from hepatoblasts. Hepatoblasts (day 9) were transduced with 3000 VP/cell of Ad-TF for 1.5 h and cultured as described in Fig. 2A. (H) On day 20, the efficiency of hepatic differentiation was measured by estimating the percentage of ASGR1-positive cells using FACS analysis. The detail results of FACS analysis are shown in Supplementary Table 1. (I) Gene expression profiles were examined on day 20. (J) Hepatoblasts (day 9) were transduced with 3000 VP/cell of Ad-TFs (in the case of combination transduction of two types of Ad vector, 1500 VP/cell of each Ad-TF was transduced) for 1.5 h and cultured. Gene expression levels of *CYP2C19* were measured by real-time RT-PCR on day 20. On the *y* axis, the gene expression level of *CYP2C19* in PHs, which were cultured for 48 h after the cells were plated, was taken as 1.0. All data are represented as mean ± SD (n = 3).

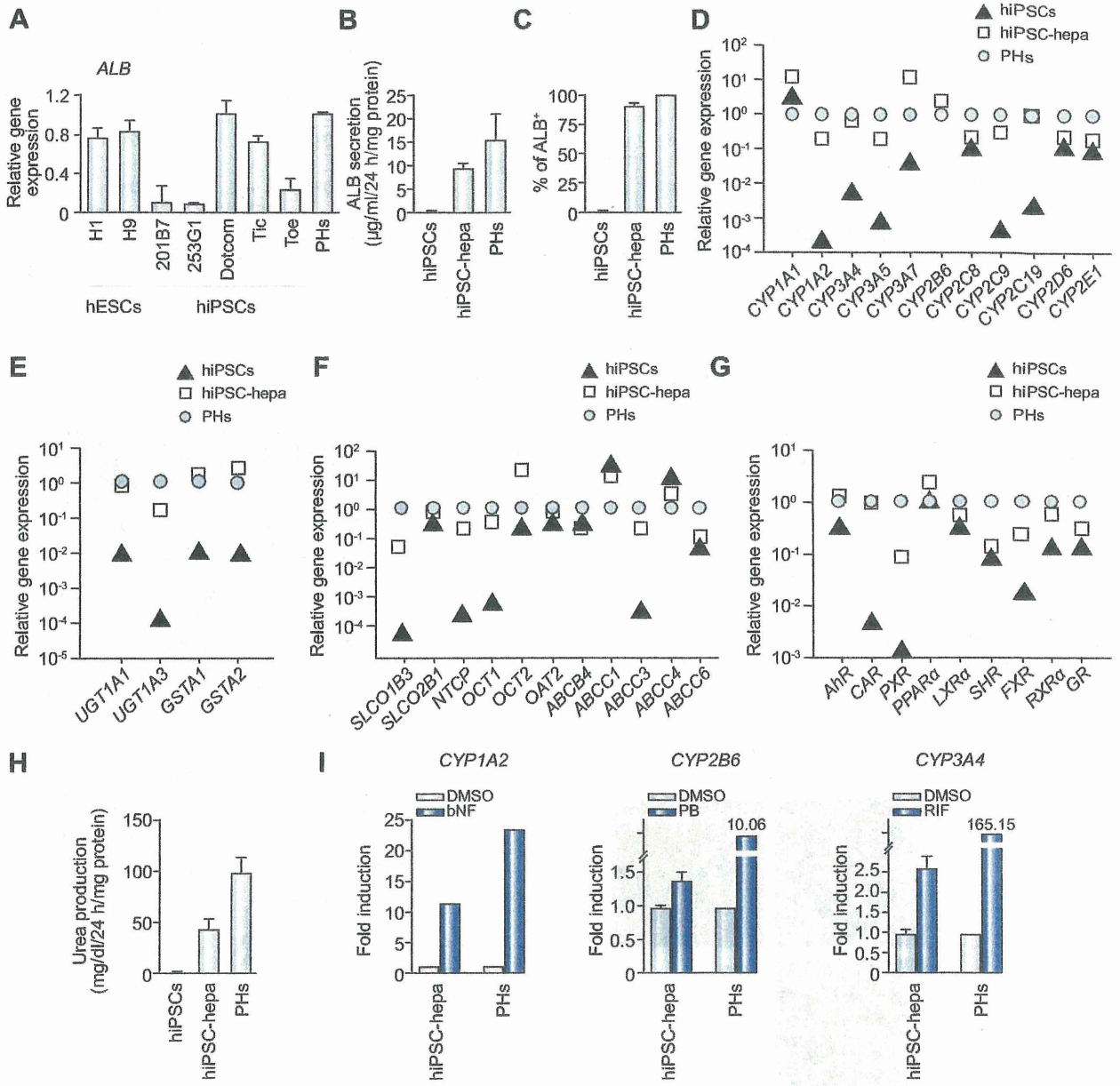

Fig. 3. The hepatic characterization of hiPSC-hepa. hESCs (H1 and H9) and hiPSCs (201B7, 253G1, Dotcom, Tic, and Toe) were differentiated into hepatocyte-like cells as described in Fig. 2A. (A) On day 20, the gene expression level of *ALB* was examined by real-time RT-PCR. On the *y* axis, the gene expression level of *ALB* in PHs, which were cultured for 48 h after cells were plated, was taken as 1.0. (B–I) hiPSCs (Dotcom) were differentiated into hepatocyte-like cells as described in Fig. 2A. (B) The amount of ALB secretion was examined by ELISA in hiPSCs, hiPSC-hepa, and PHs. (C) hiPSCs, hiPSC-hepa, and PHs were subjected to immunostaining with anti-ALB antibodies, and then the percentage of ALB-positive cells was examined by flow cytometry. (D–G) The gene expression levels of CYP enzymes (D), conjugating enzymes (E), hepatic transporters (F), and hepatic nuclear receptors (G) were examined by real-time RT-PCR in hiPSCs, hiPSC-hepa, and PHs. On the *y* axis, the expression level of PHs is indicated. (H) The amount of urea secretion was examined in hiPSCs, hiPSC-hepa, and PHs. (I) Induction of *CYP1A2*, *2B6*, or *3A4* by DMSO or inducer (bNF, PB, or RIF) of hiPSC-hepa and PHs, cultured for 48 h after the cells were plated, was examined. On the y axis, the gene expression levels of *CYP1A2*, *2B6*, or *3A4* in DMSO-treated cells, which were cultured for 48 h, were taken as 1.0. All data are represented as mean ± SD (n = 3).

dinately works to induce hepatocyte functions. Taken together, efficient hepatic differentiation could be promoted by using the combination of FOXA2 and HNF1α transduction at the optimal stage of differentiation (Fig. 2A). At the stage of hepatic expansion and maturation, Ad-HNF4α can be substituted for Ad-HNF1α (Fig. 1J). Interestingly, cell growth was delayed by FOXA2 and HNF4α transduction (Supplementary Fig. 5). This delay in cell proliferation might be due to promoted maturation by FOXA2 and HNF1α transduction. As the hepatic differentiation proceeds, the morphology of hESCs gradually changed into a typical hepatocyte morphology, with distinct round nuclei and a polygonal shape (Fig. 2B), and the expression levels of hepatic markers

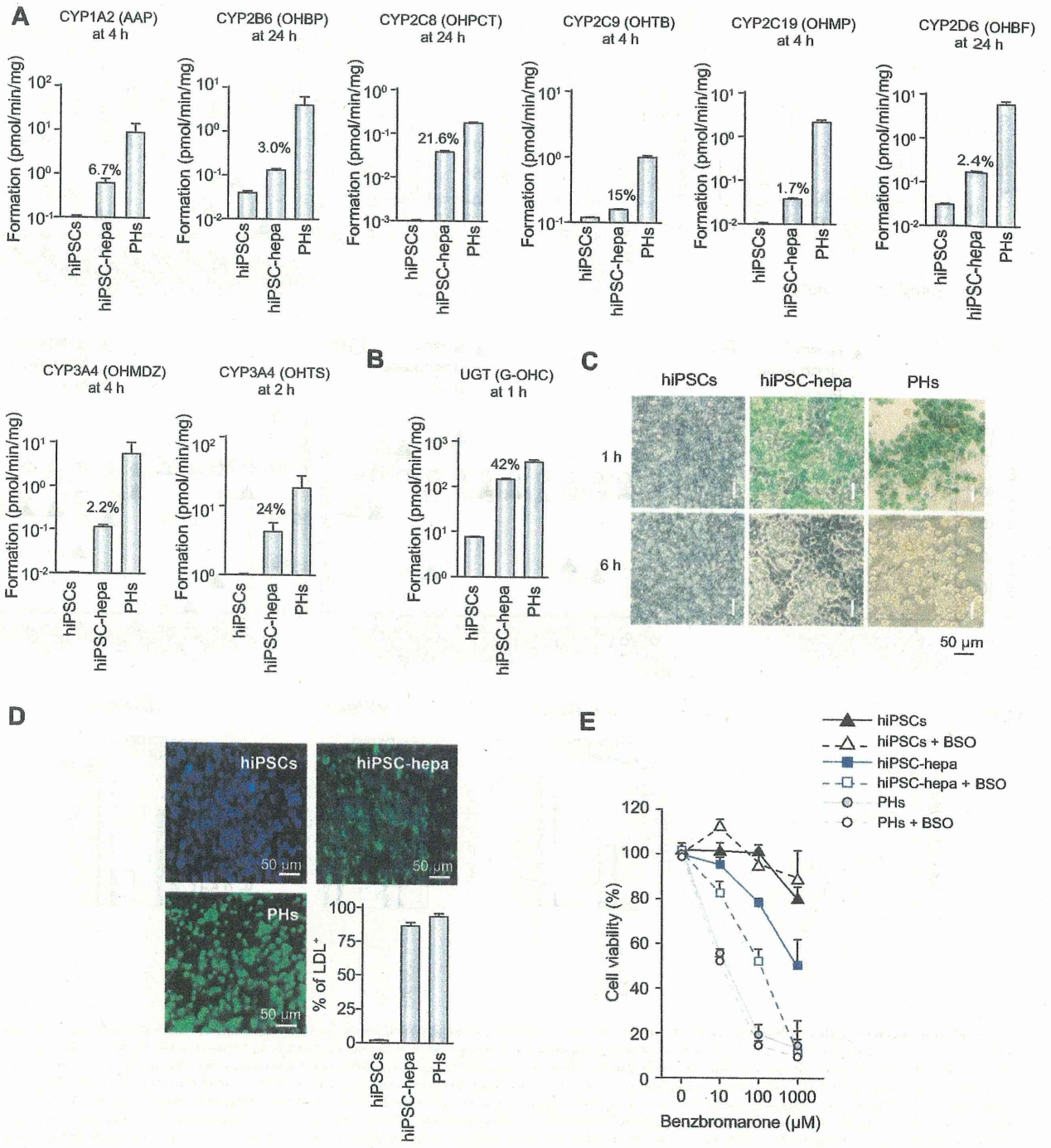

Fig. 4. Evaluation of the drug metabolism capacity and hepatic transporter activity of hiPSC-hepa. hiPSCs (Dotcom) were differentiated into hepatocytes as described in Fig. 2A. (A and B) Quantitation of metabolites in hiPSCs, hiPSC-hepa, and PHs, which were cultured for 48 h after the cells were plated, was examined by treating nine substrates (Phenacetin, Bupropion, Paclitazel, Tolbtamide, *S*-mephenytoin, Bufuralol, Midazolam, Testosterone, and Hydroxyl coumarin; these compounds are substrates for CYP1A2, 2B6, 2C8, 2C9, 2C19, 2D6, 3A4, 3A4 (A) and UGT (B), respectively), and then supernatants were collected at the indicated time. The quantity of metabolites (Acetaminophen [AAP], Hydroxybupropion [OHBP], 6α-hydroxypaclitaxel [OHPCT], Hydroxytolbutamide [OHTB], 4′-hydroxymephenytoin [OHMP], 1′-hydroxybufuralol [OHBF], 1′-hydroxymidazolam [OHMDZ], 6β-hydroxytestosterone [OHTS], 7-Hydroxycoumarin glucuronide [G-OHC], respectively) was measured by LC-MS/MS. The ratios of the activity levels in hiPSC-hepa to the activity levels in PHs rate are indicated in the graph. (C) hiPSCs, hiPSC-hepa, and PHs were examined for their ability to take up ICG (top) and release it 6 h thereafter (bottom). (D) hiPSCs, hiPSC-hepa, and PHs were cultured with medium containing Alexa-Flour 488-labeled LDL (green) for 1 h, and immunohistochemistry was performed. Nuclei were counterstained with DAPI (blue). The percentage of LDL-positive cells was also measured by FACS analysis. (E)

(ALB, CYP2D6, alpha-1-antitrypsin [αAT], CYP3A4, and CYP7A1) increased (Fig. 2C). Hepatic gene expression levels (Supplementary Fig. 6A), amount of ALB secretion (Supplementary Fig. 6B), and CYP2C9 activity level (Supplementary Fig. 6C) of Ad-FOXA2- and Ad-HNF1α-transduced cells were significantly higher than those of Ad-SOX17-, Ad-HEX-, and Ad-HNF4α-transduced cells. These results indicated that FOXA2 and HNF1α transduction promotes more efficiently hepatic differentiation than SOX17, HEX, and HNF4α transduction.

Characterization of the hESC-hepa/hiPSC-hepa

As we have previously reported [6], hepatic differentiation efficiency differs among hESC/hiPSC lines. Therefore, it is necessary to select a hESC/hiPSC line that is suitable for hepatic maturation in the case of medical applications such as drug screening. In the present study, two hESC lines and five hiPSCs lines were differentiated into hepatocyte-like cells, and then their gene expression levels of *ALB* (Fig. 3A) and *CYP3A4* (Supplementary Fig. 7A), and their CYP3A4 activities (Supplementary Fig. 7B) were compared. These data suggest that the iPSC line, Dotcom [11,12], was the most suitable for hepatocyte maturation. To examine whether the iPSC (Dotcom)-hepa has enough hepatic functions as compared with PHs, the amount of albumin (ALB) secretion (Fig. 3B) and the percentage of ALB-positive cells (Fig. 3C) were measured on day 20. The amount of ALB secretion in hiPSC-hepa was similar to that in PHs and the percentage of ALB-positive cells was approximately 90% in iPSC-hepa. We also confirmed that the gene expression levels of CYP enzymes (Fig. 3D), conjugating enzymes (Fig. 3E), hepatic transporters (Fig. 3F), and hepatic nuclear receptors (Fig. 3G) in hiPSC-hepa were similar to those of PHs, although some of them were still lower than those of PHs. Because the gene expression level of the fetal CYP isoform, *CYP3A7*, in hiPSC-hepa was higher than that of PHs, mature hepatocytes and hepatic precursors were still mixed. We have previously confirmed that Ad vector-mediated gene expression in the hepatoblasts (day 9) continued until day 14 and almost disappeared on day 18 [7]. Therefore, the hepatocyte-related genes expressed in hiPSC-hepa are not directly regulated by exogenous FOXA2 or HNF1α. Taken together, endogenous hepatocyte-related genes in hiPSC-hepa should have been upregulated by FOXA2 and HNF1α transduction.

To further confirm that hiPSC-hepa have sufficient levels of hepatocyte functions, we evaluated the ability of urea secretion (Fig. 3H) and glycogen storage (Supplementary Fig. 8). The amount of urea secretion in hiPSC-hepa was about half of that in PHs. HiPSC-hepa exhibited abundant storage of glycogen. Because CYP1A2, 2B6, and 3A4 are involved in the metabolism of a significant proportion of the currently available commercial drugs, we tested the induction of *CYP1A2*, *2B6*, and *3A4* by chemical stimulation (Fig. 3I). *CYP1A2*, *2B6*, and *3A4* are induced by β-naphthoflavone [bNF], phenobarbital [PB], or rifampicin [RIF], respectively. Although undifferentiated hiPSCs did not respond to either bNF, PB, or RIF (data not shown), hiPSC-hepa produced more metabolites in response to chemical stimulation, suggesting that inducible CYP enzymes were detectable in hiPSC-hepa (Fig. 3I). However, the induction potency of *CYP1A2*, *2B6*, and *3A4* in hiPSC-hepa were lower than that in PHs.

Drug metabolism capacity and hepatic transporter activity of hiPSC-hepa

Because metabolism and detoxification in the liver are mainly executed by CYP enzymes, conjugating enzymes, and hepatic transporters, it is important to assess the function of these enzymes and transporters in hiPSC-hepa. Among the various enzymes in liver, CYP1A2, 2B6, 2C8, 2C9, 2C19, 2D6 and 3A4, UGT are the important phase I and II enzymes responsible for metabolism. Nine substrates, Phenacetin, Bupropion, Paclitazel, Tolbtamide, *S*-mephenytoin, Bufuralol, Midazolam, Testosterone, and Hydroxyl coumarin, which are the substrates of CYP1A2, 2B6, 2C8, 2C9, 2C19, 2D6, 3A4, 3A4 (Fig. 4A), and UGT (Fig. 4B), respectively, were used to estimate the drug metabolism capacity of hiPSC-hepa compared with that of PHs. To precisely estimate the drug metabolism capacity, the amounts of metabolites were measured during the phase when production of metabolites was linear (Supplementary Fig. 9). These results indicated that our hiPSC-hepa have the capacity to metabolize these nine substrates, although the activity levels were lower than those of PHs. The hepatic functions of hiPSC-hepa were further evaluated by examining the ability to uptake Indocyanine Green (ICG) and LDL (Fig. 4C and D, respectively). In addition to PHs, hiPSC-hepa had the ability to uptake ICG and to excrete ICG in a culture without ICG for 6 h (Fig. 4C), and to uptake LDL (Fig. 4D). These results suggest that hiPSC-hepa have enough CYP enzyme activity, conjugating enzyme activity, and hepatic transporter activity to metabolize various drugs.

To examine whether our hiPSC-hepa could be used to predict metabolism-mediated toxicity, hiPSC-hepa were incubated with Benzbromarone, which is known to generate toxic metabolites, and then cell viability was measured (Fig. 4E). Cell viability of hiPSC-hepa was decreased depending on the concentration of Benzbromarone. However, cell viability of hiPSC-hepa was much higher than that of PHs. To detect drug–induced cytotoxicity with high sensitivity in hiPSC-hepa, these cells were treated with Buthionine-SR-sulfoximine (BSO), which depletes cellular GST, and result in a decrease of cell viability of hiPSC-hepa as compared with that of non-treated cells (Fig. 4E). These results indicated that hiPSC-hepa would be more useful in drug screening under a condition of knockdown of conjugating enzyme activity.

Discussion

The establishment of an efficient hepatic differentiation technology from hESCs and hiPSCs would be important for the application of hESC-hepa and hiPSC-hepa to drug toxicity screening. Although we have previously reported that sequential transduc-

The cell viability of hiPSCs, hiPSC-hepa, PHs, and their BSO-treated cells (0.4 mM BSO was pre-treated for 24 h) was assessed by Alamar Blue assay after 48-hr exposure to differe2nt concentrations of benzbromarone. The cell viability is expressed as a percentage of that in cells treated only with solvent. All data are represented as mean ± SD (n = 3).

tion of SOX17, HEX, and HNF4α into hESC-derived cells could promote efficient hepatic differentiation [7], further hepatic maturation of the hESC-hepa and hiPSC-hepa was needed for this application. To further improve the differentiation efficiency of every step of hepatic differentiation (hESC to DE cells, DE cells to hepatoblasts, and hepatoblasts to hESC-hepa), we initially performed a screening of transcription factors. In the stage of DE differentiation, FOXA2 transduction could promote the most efficient DE differentiation (Fig. 1C). In the stage of hepatic commitment, expansion, and maturation, the combination of FOXA2 and HNF1α transduction strongly promoted hepatic commitment and maturation (Fig. 1F and J), although in the stage of hepatic expansion and maturation, HNF4α transduction was as efficient as that of HNF1α (Fig. 1J). Since HNF1α is one of the target genes of HNF4α [13], the signaling through HNF4α to HNF1α would be important for efficient hepatic expansion and maturation. Considering these results together, we ascertained a pair of two transcription factors, FOXA2 and HNF1α, that could promote efficient hepatic differentiation from hESCs. In embryogenesis, the expression of FOXA2 and HNF1α is initially detected in DE or hepatoblasts, respectively and the expression levels of both FOXA2 and HNF1α are elevated as the liver develops [14,15]. Therefore, our hepatic differentiation technology, which employs FOXA2 and HNF1α transduction, might mimic the gene expression pattern during embryogenesis.

We found that the gene expression levels of CYP enzymes, conjugating enzymes, hepatic transporters, and hepatic nuclear receptors were upregulated by FOXA2 and HNF1α transduction (Fig. 3D–G). In contrast to the high expression levels of hepatocyte-related genes, CYP induction potency and the drug metabolism capacity of our hiPSC-hepa were lower than those of PHs (Figs. 3I and 4A and B). One of the possible reasons for the difference between gene expression levels of CYP enzymes and CYP induction activity might be that there were insufficient expression levels of hepatic nuclear receptors (such as *PXR*, *SHR*, and *FXR*) in hiPSC-hepa (Fig. 3G). Because many CYPs require high expression levels of hepatic nuclear receptor for efficient drug metabolism [16], transduction of these hepatic nuclear receptor genes in hiPSC-hepa or development of a differentiation method that induces high expression of these nuclear receptors might improve the drug metabolic capacity. Another explanation for the low CYP activities in hiPSC-hepa, maybe that hiPSCs were established from an individual with low CYP activities; infact, it is known that large individual differences in CYP activities are observed among individuals. It might be important to use a hiPSC line established from a person with high CYP activities. It is essential to investigate the reasons behind this significant discordance, an issue that our group is currently planning to study.

In summary, our method, consisting of sequential FOXA2 and HNF1α transduction along with the addition of adequate soluble factors at each step of differentiation, is a valuable tool for the efficient generation of functional hepatocytes derived from hESCs and hiPSCs. The hiPSC-hepa exhibited a number of hepatocyte functions (such as ALB secretion, uptake of LDL or ICG, glycogen storage, and drug metabolism capacity). In addition, the hiPSC-hepa were successfully applied to the evaluation of drug-induced cytotoxicity. Therefore, the hESC-hepa and hiPSC-hepa might be used for drug screening in early phases of pharmaceutical development.

Conflict of interest

The authors who have taken part in this study declared that they do not have anything to disclose regarding funding or conflict of interest with respect to this manuscript.

Acknowledgements

We thank Misae Nishijima, Nobue Hirata, Miki Yoshioka, and Hiroko Matsumura for their excellent technical support. We thank Ms. Ong Tyng Tyng for critical reading of the manuscript. HM, MKF, and TH were supported by grants from the Ministry of Health, Labor, and Welfare of Japan. HM was also supported by Japan Research foundation For Clinical Pharmacology, The Nakatomi Foundation, and The Uehara Memorial Foundation. K. Kawabata was supported by Grants from the Ministry of Education, Sports, Science and Technology of Japan (20200076) and the Ministry of Health, Labor, and Welfare of Japan. K. Katayama and FS were supported by Program for Promotion of Fundamental Studies in Health Sciences of the National Institute of Biomedical Innovation (NIBIO).

Supplementary data

Supplementary data associated with this article can be found, in the online version, at http://dx.doi.org/10.1016/j.jhep.2012.04.038.

References

[1] Thomson JA, Itskovitz-Eldor J, Shapiro SS, Waknitz MA, Swiergiel JJ, Marshall VS, et al. Embryonic stem cell lines derived from human blastocysts. Science 1998;282:1145–1147.
[2] Takahashi K, Tanabe K, Ohnuki M, Narita M, Ichisaka T, Tomoda K, et al. Induction of pluripotent stem cells from adult human fibroblasts by defined factors. Cell 2007;131:861–872.
[3] Clayton DF, Darnell Jr JE. Changes in liver-specific compared to common gene transcription during primary culture of mouse hepatocytes. Mol Cell Biol 1983;3:1552–1561.
[4] Snykers S, De Kock J, Rogiers V, Vanhaecke T. In vitro differentiation of embryonic and adult stem cells into hepatocytes: state of the art. Stem cells 2009;27:577–605.
[5] Inamura M, Kawabata K, Takayama K, Tashiro K, Sakurai F, Katayama K, et al. Efficient generation of hepatoblasts from human ES cells and iPS cells by transient overexpression of homeobox gene HEX. Mol Ther 2011;19:400–407.
[6] Takayama K, Inamura M, Kawabata K, Tashiro K, Katayama K, Sakurai F, et al. Efficient and directive generation of two distinct endoderm lineages from human ESCs and iPSCs by differentiation stage-specific SOX17 transduction. PLoS One 2011;6:e21780.
[7] Takayama K, Inamura M, Kawabata K, Katayama K, Higuchi M, Tashiro K, et al. efficient generation of functional hepatocytes from human embryonic stem cells and induced pluripotent stem cells by HNF4alpha transduction. Mol Ther 2012;20:127–137.
[8] Duan Y, Ma X, Zou W, Wang C, Bahbahan IS, Ahuja TP, et al. Differentiation and characterization of metabolically functioning hepatocytes from human embryonic stem cells. Stem cells 2010;28:674–686.
[9] Furue MK, Na J, Jackson JP, Okamoto T, Jones M, Baker D, et al. Heparin promotes the growth of human embryonic stem cells in a defined serum-free medium. Proc Natl Acad Sci U S A 2008;105:13409–13414.
[10] Lacroix D, Sonnier M, Moncion A, Cheron G, Cresteil T. Expression of CYP3A in the human liver–evidence that the shift between CYP3A7 and CYP3A4 occurs immediately after birth. Eur J Biochem 1997;247:625–634.

[11] Nagata S, Toyoda M, Yamaguchi S, Hirano K, Makino H, Nishino K, et al. Efficient reprogramming of human and mouse primary extra-embryonic cells to pluripotent stem cells. Genes Cells 2009;14:1395–1404.
[12] Makino H, Toyoda M, Matsumoto K, Saito H, Nishino K, Fukawatase Y, et al. Mesenchymal to embryonic incomplete transition of human cells by chimeric OCT4/3 (POU5F1) with physiological co-activator EWS. Exp Cell Res 2009;315:2727–2740.
[13] Gragnoli C, Lindner T, Cockburn BN, Kaisaki PJ, Gragnoli F, Marozzi G, et al. Maturity-onset diabetes of the young due to a mutation in the hepatocyte nuclear factor-4 alpha binding site in the promoter of the hepatocyte nuclear factor-1 alpha gene. Diabetes 1997;46:1648–1651.
[14] Ang SL, Wierda A, Wong D, Stevens KA, Cascio S, Rossant J, et al. The formation and maintenance of the definitive endoderm lineage in the mouse: involvement of HNF3/forkhead proteins. Development 1993;119:1301–1315.
[15] Kyrmizi I, Hatzis P, Katrakili N, Tronche F, Gonzalez FJ, Talianidis I. Plasticity and expanding complexity of the hepatic transcription factor network during liver development. Genes Dev 2006;20:2293–2305.
[16] Lehmann JM, McKee DD, Watson MA, Willson TM, Moore JT, Kliewer SA. The human orphan nuclear receptor PXR is activated by compounds that regulate CYP3A4 gene expression and cause drug interactions. J Clin Invest 1998;102:1016–1023.

Cell Medicine, Vol. 4, pp. 125–147, 2013
Printed in the USA.

2155-1790/13 $90.00 + .00
DOI: http://dx.doi.org/10.3727/215517912X658918
www.cognizantcommunication.com

Human Decidua-Derived Mesenchymal Cells Are a Promising Source for the Generation and Cell Banking of Human Induced Pluripotent Stem Cells

Tomoko Shofuda,* Daisuke Kanematsu,† Hayato Fukusumi,† Atsuyo Yamamoto,*
Yohei Bamba,‡ Sumiko Yoshitatsu,§ Hiroshi Suemizu,¶ Masato Nakamura,¶#
Yoshikazu Sugimoto,** Miho Kusuda Furue,†† Arihiro Kohara,‡‡ Wado Akamatsu,‡
Yohei Okada,‡§§ Hideyuki Okano,‡ Mami Yamasaki,¶¶##*** and Yonehiro Kanemura†##

*Division of Stem Cell Research, Institute for Clinical Research, Osaka National Hospital, National Hospital Organization, Chuo-ku, Osaka, Japan
†Division of Regenerative Medicine, Institute for Clinical Research, Osaka National Hospital, National Hospital Organization, Osaka, Japan
‡Department of Physiology, Keio University School of Medicine, Shinjuku-ku, Tokyo, Japan
§Department of Plastic Surgery, Osaka National Hospital, National Hospital Organization, Osaka, Japan
¶Biomedical Research Department, Central Institute for Experimental Animals, Kawasaki-ku, Kawasaki, Japan
#Department of Pathology and Regenerative Medicine, Tokai University School of Medicine, Isehara, Kanagawa, Japan
**Division of Chemotherapy, Faculty of Pharmacy, Keio University, Minato-ku, Tokyo, Japan
††Laboratory of Stem Cell Cultures, Laboratory of Cell Cultures, Department of Disease Bioresources Research, National Institute of Biomedical Innovation, Ibaraki, Osaka, Japan
‡‡JCRB Cell Bank, Laboratory of Cell Cultures, Research on Disease Bioresources, National Institute of Biomedical Innovation, Osaka, Japan
§§Kanrinmaru-Project, School of Medicine, Keio University, Tokyo, Japan
¶¶Division of Molecular Medicine, Institute for Clinical Research, Osaka National Hospital, National Hospital Organization, Osaka, Japan
##Department of Neurosurgery, Osaka National Hospital, National Hospital Organization, Osaka, Japan
***Department of Pediatric Neurosurgery, Takatsuki General Hospital, Takatsuki, Osaka, Japan

Placental tissue is a biomaterial with remarkable potential for use in regenerative medicine. It has a three-layer structure derived from the fetus (amnion and chorion) and the mother (decidua), and it contains huge numbers of cells. Moreover, placental tissue can be collected without any physical danger to the donor and can be matched with a variety of HLA types. The decidua-derived mesenchymal cells (DMCs) are highly proliferative fibroblast-like cells that express a similar pattern of CD antigens as bone marrow-derived mesenchymal cells (BM-MSCs). Here we demonstrated that induced pluripotent stem (iPS) cells could be efficiently generated from DMCs by retroviral transfer of reprogramming factor genes. DMC-hiPS cells showed equivalent characteristics to human embryonic stem cells (hESCs) in colony morphology, global gene expression profile (including human pluripotent stem cell markers), DNA methylation status of the OCT3/4 and NANOG promoters, and ability to differentiate into components of the three germ layers in vitro and in vivo. The RNA expression of XIST and the methylation status of its promoter region suggested that DMC-iPSCs, when maintained undifferentiated and pluripotent, had three distinct states: (1) complete X-chromosome reactivation, (2) one inactive X-chromosome, or (3) an epigenetic aberration. Because DMCs are derived from the maternal portion of the placenta, they can be collected with the full consent of the adult donor and have considerable ethical advantages for cell banking and the subsequent generation of human iPS cells for regenerative applications.

Key words: Induced pluripotent stem cells (iPSCs); Decidua; Mesenchymal cells; X-chromosome inactivation

INTRODUCTION

Great breakthroughs in cell reprogramming technology have led to the generation of induced pluripotent stem cells (iPSCs) and dramatic advances in stem cell research (43). To date, iPSCs have been generated efficiently from various accessible human tissues, including

Received May 31, 2012; final acceptance September 30, 2012. Online prepub date: November 1, 2012.
Address correspondence to Yonehiro Kanemura, M.D., Ph.D., Division of Regenerative Medicine, Institute for Clinical Research, Osaka National Hospital, National Hospital Organization, 2-1-14 Hoenzaka, Chuo-ku, Osaka 540-0006, Japan.
Tel: +81-6-6942-1331; Fax: +81-6-6946-3530; E-mail: kanemura@onh.go.jp

dermal fibroblasts (22,27,37,42,47), blood cells (9,10,21), neural stem cells (6,19), mesenchymal stem cells (MSCs) (4,33,35), and keratinocytes (1). It is generally accepted that iPSCs are likely to contribute not only to the realization of regenerative medicine through the use of pluripotent stem cells but also to the elucidation of the molecular pathogenesis of many intractable diseases. The promise of therapies using human iPSCs (hiPSCs) has driven an intense search for good cell sources (34).

Human placenta is a fetal adnexal tissue that contains extraembryonic cells. It is composed of three layers: the amnion and the chorion, which are of fetal origin, and the decidua, which is of maternal origin. Fibroblast-like adherent cells isolated from various components of the fetal adnexa, including the placenta, show multipotency or pluripotency, suggesting that the fetal adnexa represents a new source of human stem cells (3,8,14,46). We recently isolated adherent cells from human term decidua vera, that is, decidua-derived mesenchymal cells (DMCs), and reported some of their properties (18). DMCs are highly proliferative fibroblast-like cells of purely maternal origin, and they express a similar pattern of cluster of differentiation (CD) antigens as bone marrow-derived mesenchymal cells (BM-MSCs). DMCs differentiate well into chondrocytes and moderately into adipocytes, but hardly at all into osteoblasts, in vitro (18). The high-proliferative ability of DMCs makes them relatively easy to prepare and maintain, and their derivation from the maternal portion of the human placenta, which is otherwise discarded, resolves many ethical concerns. These unique properties of DMCs give them several advantages for clinical use, and support their potential as an attractive alternative to allogeneic human stem cells for use in regenerative medicine (15,18).

In this study, we asked whether DMCs could be reprogrammed into hiPSCs and acquire pluripotency. The four reprogramming factors octamer-binding transcription factor 3/4 (OCT3/4), sex-determining region Y box 2 (SOX2), Krüppel-like factor 4 (KLF4), and myelocytomatosis viral oncogene homolog (MYC; OSKM), carried by retroviral vectors (42), were used to reprogram several lines of DMCs. The resulting hiPSCs closely resembled human embryonic stem cells (hESCs) in their morphology, and they expressed hESC markers, which are low or undetectable in native DMCs. These hiPSCs formed embryoid bodies in vitro and teratomas in vivo that contained components of all three germ layers. We think these unique properties of DMCs give them several advantages for clinical use and that the generation of hiPSCs from DMCs could lead to the establishment of hiPSC-banking systems. Such systems would increase the availability of allogeneic hiPSCs, because tissues expressing a wide array of human leukocyte antigen (HLA) variants could be banked for clinical applications.

MATERIALS AND METHODS

Human Tissues and Cells

This study was carried out in accordance with the principles of the Helsinki Declaration, and approvals to use human tissues were obtained from the ethical committee of Osaka National Hospital (No. 72, No. 109, and No. 110). The donor bloods were serologically tested for hepatitis B and C, human immunodeficiency virus (HBs, HCV, HIV), and syphilis. Full-term placental tissues, infant skin samples obtained during plastic surgery, and the results of donor blood tests were collected at the Osaka National Hospital with written informed consent.

Human ESCs (clone KhES1) were obtained from Kyoto University (Kyoto, Japan) (41) and propagated at Keio University in accordance with Japanese guidelines on the utilization of hESCs, under approval of the Ministry of Education, Culture, Sports, Science and Technology (MEXT) of Japan and the ethical committee of Keio University. Human iPSCs (clone 201B7) (42) were obtained from the RIKEN Cell Bank (Tsukuba, Japan).

Human Primary Cell Culture

Human DMCs were propagated from human term decidua vera, in Dulbecco's modified Eagle's medium (DMEM)/F-12 (1:1) supplemented with 10% fetal bovine serum (FBS), HEPES (15 mM), and antibiotic–antimycotic solution (Invitrogen, Carlsbad, CA, USA) at 37°C in 5% CO_2 as previously described (18,28). Human amnion-derived epithelial cells (AECs), human amnion-derived mesenchymal cells (AMCs), and human primary BM-MSCs were also propagated as previously described (18). Human primary dermal fibroblast cells (DFBs) were isolated from the toe skin tissue of infants with polydactyly and cultured in DMEM/F-12 (1:1) with 10% fetal bovine serum (FBS).

Generation and Culture of hiPSCs

Four pMX retroviral vectors encoding the reprogramming factors (OSKM) were obtained from Addgene, Inc. (Cambridge, MA, USA) (42). Amphotropic retroviruses were produced by the transfection of Platinum-A retroviral packaging cells (Cell Biolabs, Inc., San Diego, CA, USA) using FuGENE® 6 Transfection Reagent (Roche Diagnostics, Indianapolis, IN, USA). Host cells were infected with the retrovirus supernatants supplemented with polybrene (4 mg/ml, Nacalai Tesque, Kyoto, Japan). On day 5 postinfection, the cells were replated on mitomycin C-treated mouse embryonic fibroblast (MEF) feeder cells at a density of 2.5×10^4 cells/6-cm-diameter culture dish or 5×10^5 cells/10-cm culture dish. On the next day, the growth medium was replaced with hESC medium consisting of DMEM/F-12 (1:1) with 20% knockout serum replacement (KSR, Invitrogen)/2-mercaptoethanol (1 mM; Invitrogen)/basic fibroblast growth factor (bFGF; 5 ng/ml;

Wako Pure Chemical Industries, Ltd., Osaka Japan). The number of alkaline phosphatase (ALP)$^+$ colonies in a 6-cm culture dish was screened and estimated by staining with 1-Step™ NBT/BCIP reagent (Pierce Biotechnology, Rockford, IL, USA), according to the manufacturer's specifications at 28 days postinfection. Concurrently, human ESC-like colonies grown in the 10-cm culture dish were picked up around 30 days after gene induction. The colonies were clonally expanded for further analyses. Human ES cells (KhES1) and hiPSCs (201B7) were also propagated on feeder cells with hESC medium (41).

Quantitative Reverse Transcription-Polymerase Chain Reaction (qRT-PCR)

Total RNA was isolated using an RNeasy Mini kit (Qiagen, Valencia, CA, USA), and cDNAs were synthesized using a PrimeScript® First-Strand Synthesis Kit (Takara Bio, Inc., Shiga, Japan), according to the manufacturer's specifications. Quantitative PCR analysis was performed using gene-specific primers (Table 1) with Power SYBR® Green PCR Master Mix and the 7300 real-time PCR system (Applied Biosystems, Foster, CA, USA), and the comparative Ct or standard curve method

Table 1. Primers Used for RT-PCR and PCR

Description and Genes	Symbol	Gene ID		Primer Sequence (5′ to 3′)
Transgene detection				
POU class 5 homeobox 1	OCT3/4Tg	5460	S	CCCCAGGGCCCCATTTTGGTACC
			A	TTATCGTCGACCACTGTGCTGCTG
SRY (sex-determining region Y)-box 2	SOX2Tg	6657	S	GGCACCCCTGGCATGGCTCTTGGCTC
			A	TTATCGTCGACCACTGTGCTGCTG
v-Myc myelocytomatosis viral oncogene homolog	MYCTg	4609	S	CAACAACCGAAAATGCACCAGCCCCAG
			A	TTATCGTCGACCACTGTGCTGCTG
Krüppel-like factor 4	KLF4Tg	9314	S	ACGATCGTGGCCCCGGAAAAGGACC
			A	TTATCGTCGACCACTGTGCTGCTG
Expression of hES markers				
POU class 5 homeobox 1	OCT3/4	5460	S	GACAGGGGGAGGGGAGGAGCTAGG
			A	CTTCCCTCCAACCAGTTGCCCCAAAC
SRY (sex-determining region Y)-box 2	SOX2	6657	S	GGGAAATGGGAGGGGTGCAAAAGAGG
			A	TTGCGTGAGTGTGGATGGGATTGGTG
v-Myc myelocytomatosis viral oncogene homolog	MYC	4609	S	GCGTCCTGGGAAGGGAGATCCGGAGC
			A	TTGAGGGGCATCGTCGCGGGAGGCTG
Krüppel-like factor 4	KLF4	9314	S	ACGATCGTGGCCCCGGAAAAGGACC
			A	TGATTGTAGTGCTTTCTGGCTGGGCTCC
Nanog homeobox	NANOG	79923	S	GCAGAAGGCCTCAGCACCTA
			A	GGTTCCCAGTCGGGTTCAC
Telomerase reverse transcriptase	TERT	7015	S	CTCCATCCTGAAAGCCAAGAA
			A	CGAGTCAGCTTGAGCAGGAA
X (inactive)-specific transcript (nonprotein coding)	XIST	7503	S	TGGCAGGGAGTGCCAGCTCCA
			A	GACCAAGGTGCATGGCTGCGGT
Expression of endoderm markers				
Forkhead box A2	FOXA2	3170	S	TGCTGGTCGTTTGTTGTGG
			A	CATGTTGCTCACGGAGGAGTAG
GATA binding protein 4	GATA4	2626	S	CTCTTCAGGCAGTGAGAGCC
			A	GGTCCGTGCAGGAATTTGAGG
SRY (sex-determining region Y)-box 17	SOX17	64321	S	CCCATAGTTGGATTGTCAAAACC
			A	CACACCCAGGACAACATTTCTTT
α-Fetoprotein	AFP	174	S	TTGAGAAACCCACTGGAGATGA
			A	GTTATGTCTTCCCTCTTCACTTTGG
Albumin	ALB	213	S	GTTGCATGAGAAAACGCCAGTA
			A	AGCATGGTCGCCTGTTCAC
Expression of mesoderm markers				
T, brachyury homolog (mouse)	Brachyury	6862	S	TGGAATGCCTGCCCATC
			A	CCGTTGCTCACAGACCACA

(*continued*)

Table 1. Primers Used for RT-PCR and PCR (*Continued*)

Description and Genes	Symbol	Gene ID		Primer Sequence (5′ to 3′)
NK2 transcription factor related, locus 5	NKX2-5	1482	S	CCCCTGGATTTTGCATTCAC
			A	CGTGCGCAAGAACAAACG
Msh homeobox 1	MSX1	4487	S	CAGAAGATGCGCTCGTCAAA
			A	CGGCTTACGGTTCGTCTTG
Collagen, type II, α1	COL2A1	1280	S	GGAAGAGTGGAGACTACTGGATTGAC
			A	TCCATGTTGCAGAAAACCTTCA
Expression of neural markers				
Neurogenin 2	NEUROG2	63973	S	ATGCCTATTGTCCTGTCCTTCTCT
			A	TGACTTCTAACCTGCCCCTCTAAC
SRY (sex-determining region Y)-box 1	SOX1	6656	S	AGCAGTTGTTTCTGGAAGAGTCTGT
			A	AGGCCCTTATCCCGGACTAA
Paired box 6	PAX6	5080	S	ACCTGGCTAGCGAAAAGCAA
			A	CCCGTTCAACATCCTTAGTTTATCA
Expression of astrocyte marker				
Glial fibrillary acidic protein	GFAP	2670	S	ACATCGAGATCGCCACCTAC
			A	ACATCACATCCTTGTGCTCC
Expression of Epidermis marker				
Keratin 17	KRT17	3872	S	AGGAGATTGCCACCTACCG
			A	CTTGCCATCCTGGACCTCTT
Expression of other genes				
v-Myc myelocytomatosis viral oncogene homolog 1, lung carcinoma derived	MYCL1	4610	S	CGAGAGCCCAAGCGACTCGGAGAA
			A	CAGGGGGTCTGCTCGCACCG
GLIS family zinc finger 1	GLIS1	148979	S	TCTGCCCAGCCCACAAGGTTACCA
			A	GGCAGCGCTGTGGGGCATGA
GLIS family zinc finger 2	GLIS2	84662	S	CCGCTGTCCGACCTGCAGCA
			A	GGCTTCTCACCTGTGTGCGACCG
GLIS family zinc finger 3	GLIS3	169792	S	TGCTCACCAATGGGAAGCCGCG
			A	AGCCAAGAGCCCCTTTCCCAGGAT
Zinc finger and SCAN domain containing 4	ZSCAN4	201516	S	TCCACCTGCCTTAGTCCACGTCCA
			A	TGGGAGGGTGTCCCCATGTTTGCT
Internal control				
Glyceraldehyde-3-phosphate dehydrogenase	GAPDH	2597	S	CCACTTTGTCAAGCTCATTTCCT
			A	TCTCTTCCTCTTGTGCTCTTGCT
Bisulfite genomic sequencing PCR				
Nanog homeobox promoter	Bis-NANOG P	79923	S	GTTGGGTTTGTTTTTAGGTTTT
			A	CATAAAAACAACCAACTCAATCC
POU class 5 homeobox 1 promoter	Bis-OCT3/4 P	5460	S	GTTAAGGTTAGTGGGTGGGATT
			A	AACATAAAAAAATCCCCCACA
Methylation-specific PCR				
Unmethylated-XIST promoter	Unmet-XIST P	7503	S	TTTTGTTGTAGTGTTTAAGTGGT
			A	AACCCACCATATTTTACACTACA
Methylated-XIST promoter	Met-XIST P	7503	S	TGTCGTAGTGTTTAAGTGGC
			A	CCGCCATATTTTACACTACG

S, sense primer; A, antisense primer.

(20). Total RNA isolated from various human tissues was used for controls (BD Biosciences, San Jose, CA, USA).

Microarray Analysis

The microarray study was carried out using the GeneChip array (Human Genome U133 Plus 2.0 gene expression array, Affymetrix, Inc., Santa Clara, CA, USA). One hundred nanograms of total RNA was used to synthesize amplified RNA (aRNA) using the 3′ IVT Express Kit, according to the manufacturer's instructions (Affymetrix). After aRNA purification, 15 μg of aRNA was fragmented and hybridized with a preequilibrated GeneChip array at 45°C for 16 h. The GeneChip array was then washed, stained, and scanned according to the manufacturer's instructions. The gene expression data were extracted using Affymetrix Expression Console software, and the

data sets were analyzed using GeneSpring GX software (Agilent Technologies, Inc., Santa Clara, CA, USA).

Flow cytometry (FCM) Analysis

Cells were preincubated with Y-27632 (Wako Pure Chemical Industries, Ltd.) for 30 min and then dissociated by trypsin/EDTA (Invitrogen). The dissociated cells were fixed with 4% paraformaldehyde (PFA) for 20 min on ice, washed with PBS, and then reacted with the following primary antibodies (Abs) for 30 min at 4°C: anti-stage-specific embryonic antigen 4 (SSEA-4) Ab (MC-813-70, Chemicon International, Inc., Temecula, CA, USA), anti-SSEA-3 Ab (MC-631, Chemicon), anti-TRA-1-60 Ab (TRA-1-60, Chemicon), or anti-TRA-1-81 Ab (TRA-1-81, Chemicon). After being washed, the cells were incubated with the appropriate secondary Abs (Alexa 488-conjugated anti-mouse IgG, anti-mouse IgM, or anti-rat IgM, Molecular Probes, Invitrogen) for 30 min at 4°C. The stained samples were analyzed by a FACSCalibur™ flow cytometer (BD Biosciences). All stainings were performed with matched-isotype controls.

Karyotype Analysis

Cells were cultured with colcemid (0.06 μg/ml; Invitrogen) at 37°C for 4 h, treated with Y-27632 to prevent apoptosis, and then dissociated with 0.05% trypsin/EDTA. The cells were incubated in KCl solution (75 mM) for 20 min and then fixed in Carnoy fluid. The fixed samples were heat-denatured at 95°C for 2 h, incubated in 0.025% trypsin for 10 s, and then stained with Giemsa (Merck, Darmstadt, Germany) for 7 min. The samples were observed with a microscope (Carl Zeiss, Hallbergmoos, Germany), and metaphase samples were analyzed using Ikaros (MetaSystems, Altlussheim, Germany).

Genotyping of Short-Tandem Repeat (STR) Polymorphisms

Genomic DNA (gDNA) was extracted by DNAzol Reagent (Invitrogen). STR loci were analyzed with the Powerplex 16 system (Promega, Madison, WI, USA) using an ABI PRISM3100 Genetic Analyzer (Applied Biosystems) and analyzed by GeneMapper software (Applied Biosystems) following the manufacturer's instructions (18).

Bisulfite Modification, DNA Sequencing, and Methylation-Specific PCR (MSP)

Genomic DNA was bisulfite-treated with an EZ DNA methylation-Gold Kit (Zymo Research, Irvine, CA, USA) according to the manufacturer's instructions. The promoter regions of human OCT3/4 and NANOG were amplified with specific primer sets (Table 1) by TaKaRa Taq™ Hot Start Version (Takara Bio, Inc.). The PCR products were subcloned into the pCR®2.1 vector (Invitrogen). Ten clones were sequenced with a universal primer using an ABI PRISM 3100 Genetic Analyzer (Applied Biosystems) and analyzed with Sequence analysis software (Applied Biosystems), following the manufacturer's instructions. Episcope® Methylated and Unmethylated HCT116 gDNA (Takara Bio, Inc.) were used as the control human genomic DNAs for the methylation analysis.

In Vitro Differentiation

Cells were incubated with 1 mg/ml collagenase type IV (Invitrogen) for 5 min at 37°C and harvested by scraper. The harvested colonies were broken into properly sized clumps by pipetting and then incubated on noncoated plates in human ES cell medium without bFGF to form embryoid bodies (EBs). After 10 days in floating culture, the EBs that formed were harvested for transcript analysis. Some of the EBs were transferred to gelatin-coated chamber slides (Nalge Nunc International, Rochester, NY, USA) and cultured for another 2 weeks (total 24 days) in DMEM supplemented with 10% FBS at 37°C in 5% CO_2.

Teratoma Formation Assay

NOG (non-obese diabetic/Shi-severe combined immunodeficient interleukin 2 receptor γ chain null; NOD/Shi-scid IL2Rγ null) mice (16) aged 6–8 weeks were maintained under specific pathogen-free conditions in the Animal Facility of the Central Institute for Experimental Animals (CIEA) in accordance with the guidelines of the Animal Care Committee at CIEA. All mouse studies were approved by the Animal Care Committee at CIEA. The recipient mice were anesthetized by isoflurane inhalation (Dainippon Pharmaceutical Co., Ltd., Osaka, Japan). Human iPSCs were transplanted into both subcutaneous tissue and kidney capsules. For the subcutaneous transplantation, hiPSCs (1×10^6 cells/0.1 ml of serum-free medium) were injected subcutaneously into the flank. For transplantation into the kidney capsule, the kidney was exteriorized through a dorsal–horizontal incision. A syringe fitted with a 29-G needle with a flattened tip was used. The needle was introduced into the kidney at a site apart from the transplanted region. The kidney was penetrated, and the tip of the needle was held just beneath the renal capsule. The suspension of hiPSCs (1×10^5 cells/10 μl of serum-free medium) was then injected underneath the kidney capsule. The mice were examined daily, and tumors were measured with calipers.

Teratoma samples were dissected and fixed with 4% (v/v) phosphate-buffered formalin, and paraffin-embedded sections were stained with hematoxylin and eosin using routine procedures (H&E staining).

Immunocytochemical and Immunohistochemical Staining

Cultured cells were fixed in 4% PFA, and tissue specimens were permeabilized with 0.1% Triton X-100. Nonspecific reactions were blocked with 10% normal goat serum. The samples were reacted with the following Abs overnight at 4°C: anti-α-fetoprotein (AFP) Ab (SantaCruz, Santa Cruz, CA, USA), anti-cytokeratin19 Ab (clone A53-B/A2, Santa Cruz), anti-desmin Ab (Thermo, Waltham, MA, USA), anti-α-smooth muscle actin (SMA) Ab (clone 1A4, Dako, Glostrup, Denmark), anti-glial fibrillary acidic protein (GFAP) Ab (Sigma, St. Louis, MO, USA), anti-βIII-tubulin Ab (clone TuJ1, Babco, Richmond, CA, USA), anti-vimentin Ab (Chemicon), anti-OCT3/4 Ab (Chemicon), and anti-NANOG Ab (Reprocell, Tokyo, Japan). The samples were then reacted with the appropriate secondary Abs (AlexaFluor®-488-conjugated goat anti-mouse IgG Ab, AlexaFluor®-568-conjugated goat anti-rabbit IgG Ab, Molecular Probes, Invitrogen), and TO-PRO-3® iodide (1 mM, Molecular Probes, Invitrogen) for 1 h at room temperature (RT).

The immunohistochemical staining of teratoma samples was carried out using an automated staining device with the Bond™ Polymer Refine Detection system (Leica Microsystems K.K., Tokyo, Japan) according to the manufacturer's instructions with minor modifications. In brief, 4-μm sections of formalin-fixed, paraffin-embedded tissues were deparaffinized with Bond™ Dewax Solution (Leica Microsystems), and antigen retrieval was performed using Bond™ ER Solution (Leica Microsystems) for 30 min at 100°C. Nonspecific peroxidase activity was quenched by incubating with 0.3% hydrogen peroxide for 5 min. The sections were incubated for 15 min at ambient temperature with the following Abs: anti-cytokeratin Ab (AE1/AE3, Leica Microsystems), anti-neural cell adhesion molecule (NCAM; CD56) Ab (1B6, Nichirei Bioscience, Tokyo, Japan), anti-desmin Ab (D33, Nichirei Bioscience), for 1 h at room temperature. The signals were detected by Bond™ Polymer Refine Detection (Leica Microsystems) with 3,3′-diaminobenzidine tetrahydrochloride (DAB; Dojindo Laboratories, Kumamoto, Japan) substrate as the chromogen. The sections were counterstained with hematoxylin.

The immune-stained preparations were examined using a confocal laser scanning microscope (LSM510, Carl Zeiss) or a light microscope (IX70, Olympus, Tokyo, Japan). All stainings were performed with matched isotype controls.

Statistical Analysis

Significant differences in the gene expression levels obtained by qRT-PCR were determined by analysis of variance (ANOVA) with post hoc comparisons. Details are provided in the figure legends.

RESULTS

Phenotype Analysis of Human Placenta-Derived Cells

To learn whether hiPSCs could be generated from placenta-derived cells by introducing retroviruses expressing the four reprogramming factors (OSKM), we first propagated three different kinds of somatic cells, DMCs, AECs, and AMCs, from human full-term placenta tissue (Fig. 1A) (18) and analyzed their endogenous expression of six pluripotent cell-specific marker genes in comparison with hESCs (KhES1), human primary DFBs, and human primary BM-MSCs (Fig. 1B). Quantitative RT-PCR analysis showed that c-MYC was expressed endogenously in all six cell types at the same level or higher than in hESCs and that the KLF4 levels were about the same in every cell type except DMCs (Fig. 1B). In contrast, the expression levels of the other four genes in five cell types (DFBs, AECs, AMCs, DMCs, and BM-MSCs) were significantly lower than in KhES1, to differing degrees (Fig. 1B).

Although AECs expressed higher levels of OCT3/4, NANOG, and SOX2 than the other four cell types (Fig. 1B) and thus seemed likely to be good candidate cells for generating hiPSCs (17), their growth was too slow (18) for them to be efficiently infected by retroviral vectors, and they were therefore excluded from further examination in this study.

Generation of iPSCs From Human DMCs

We next examined the gene transduction efficiency by amphotropic retrovirus infection. Three human primary cell types (DFBs, AMCs, and DMCs) were transduced with amphotropic retroviruses encoding the four reprogramming factors (OSKM), and OSKM transgene expression on day 3 postinfection was quantified by qRT-PCR (Fig. 2A). The expression of the exogenous reprogramming factors was two to three times higher in DMCs than DFBs ($p<0.01$) (Fig. 2A), and AMCs showed a comparable or lower expression than DFBs ($p<0.05$). On day 5 postinfection, the cells were split and replated on feeder cultures, and on day 28 postinfection, the reprogramming efficiency of each cell type was estimated by the number of ALP^+ (primary) colonies on 6-cm culture dishes. Approximately three times more primary colonies were generated from DMCs than AMCs, although the number was still half that generated from DFBs (Fig. 2B, top).

iPSCs of each cell type were generated from two 10-cm dishes containing 1×10^5 cells, infected as described above. The efficiency of hESC-like colony formation was determined by dividing the number of colonies with ESC-like morphology that emerged on the dishes by the number of seeded cells. The efficiency was

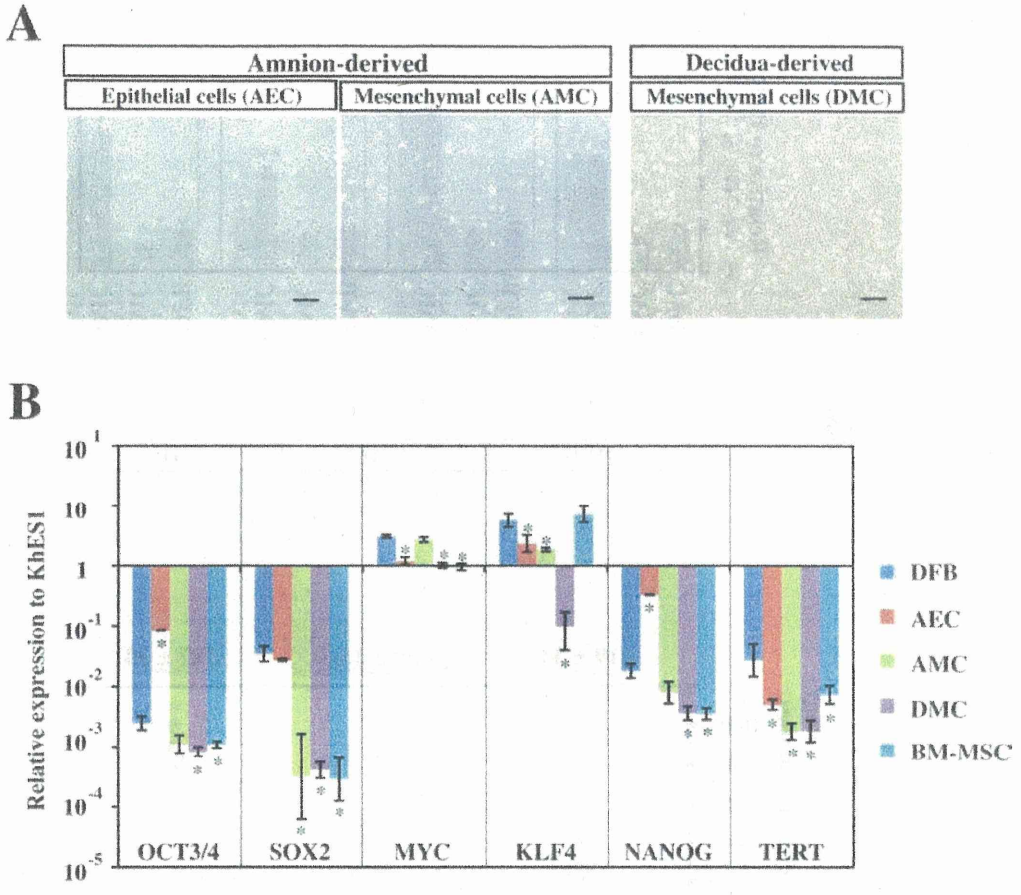

Figure 1. Phenotype analysis of human placenta-derived cells. (A) Phase contrast images of amnion-derived epithelial cells (AECs), amnion-derived mesenchymal cells (AMCs), and decidua-derived mesenchymal cells (DMCs). Scale bars: 200 μm. (B) Endogenous transcriptional expression of four reprogramming factors (OCT3/4, SOX2, KLF4, c-MYC) and pluripotent stem cell marker genes (NANOG and TERT). GAPDH was used as the internal control gene, and data are presented as the mean ± SD ($n=3$). Statistical significance was determined by Scheffe's test after ANOVA, and the p values between dermal fibroblast cells (DFBs) and other cells are shown (*$p<0.01$). See Table 1 for gene definitions. BM-MSCs, bone marrow-derived mesenchymal cells.

0.009 ± 0.002% for DFBs (mean ± SE, five independent experiments with five DFB lines), 0.020 ± 0.008% for AMCs (three independent experiments with two AMC lines), and 0.005 ± 0.001% for DMCs (12 experiments with eleven DMC lines), respectively.

We also examined the cellular properties of the morphologically hESC-like colonies generated on 10-cm culture dishes, as candidates for further analysis. After they were subcultured, approximately 90% of the colonies derived from primary colonies of DMCs retained both their hESC-like morphology and positive ALP activity after the second passage, whereas only 40% of the colonies from AMCs and DFBs met both conditions (Fig. 2B, bottom). Based on these findings, we selected DMCs as the first cells to use for iPSC generation.

Cellular Properties of DMC-hiPSCs

The DMC-hiPSC clones that retained their hESC-like morphology and positive ALP activity after several passages were also confirmed to express NANOG protein by immunocytochemistry (Fig. 3A). Expression analysis of the four transgenes by qRT-PCR analysis showed that each transgene was almost completely suppressed in two representative DMC-hiPSC clones (DMC5403 and DMC5413) compared with those on day 3 postinfection (Fig. 3B). To evaluate the protein levels of hESC markers, we analyzed two established clones and their parental DMCs (DMC54) by FCM. This analysis revealed that the two established clones highly expressed hESC-specific surface antigens (SSEA-3, SSEA-4, TRA-1-60, and TRA-1-81), whereas the parental DMCs showed little or

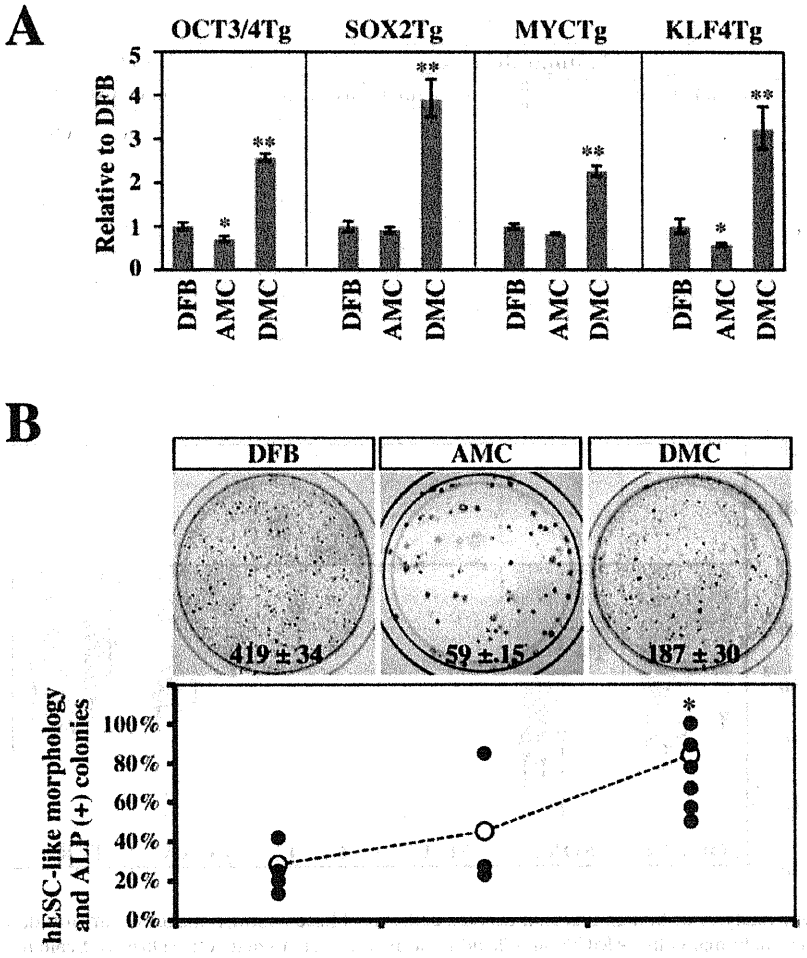

Figure 2. Efficiencies of gene transduction and generation of alkaline phosphatase (ALP)$^+$ colonies. (A) Gene transduction efficiencies of amphotropic retrovirus infection. Efficiencies were estimated on day 3 postinfection by qRT-PCR and are shown in comparison with those in DFBs (mean±SD, 3 independent experiments). Statistical significance was determined by Scheffe's test after ANOVA (*$p<0.05$, **$p<0.01$). (B) Generation efficiency of ALP$^+$ colonies. (Top) Representative result of ALP$^+$ primary colonies (blue) emerging from 2.5×10^4 infected cells on a 6-cm culture dish (mean±SD, 3 independent experiments). (Bottom) Efficiencies of retention of both the human embryonic stem cell (hESC)-like morphology and ALP activity in secondary colonies. Efficiency was determined by dividing the number of secondary colonies by the number of primary hESC-like colonies emerged on two 10-cm dishes. ●Independent results from 5 DFB experiments (DFB01, DFB18, DFB22, DFB37, and DFB44), 3 AMC experiments (AMC41 and a duplicate of AMC49), and 12 DMC experiments (DMC41 and duplicates of DMC54, DMC70, DMC71, DMC72, DMC73, DMC75, DMC76, DMC77, DMC83, and DMC92). ○Mean value. Statistical significance was determined by Scheffe's test after ANOVA (*$p<0.01$). See Table 1 for gene definitions.

no expression of these antigens, in comparison with the isotypic control antibody samples (Fig. 3C).

Karyotyping, Genotyping, and Promoter Methylation Analysis

Karyotyping by G band staining showed that both DMC-hiPSC clones had a normal female karyotype (46, XX) (Fig. 4A). Analysis of the methylation state of the OCT3/4 and NANOG promoters revealed that most of the CpG sites in the DMC-hiPSC clones were unmethylated, while those of the parental DMCs were highly methylated (Fig. 4B). Genotyping by STR-PCR showed a complete match of STRs between the parental DMCs and the two established clones (Table 2). These findings confirmed that the two DMC-hiPSC clones were derived from the parental DMCs and that their epigenetic status had been reprogrammed efficiently.

In Vitro Differentiation of DMC-hiPSCs

To confirm that the DMC-hiPSCs were pluripotent in vitro, we performed EB formation assays. The DMC-hiPSCs formed EBs in a 10-day suspension culture

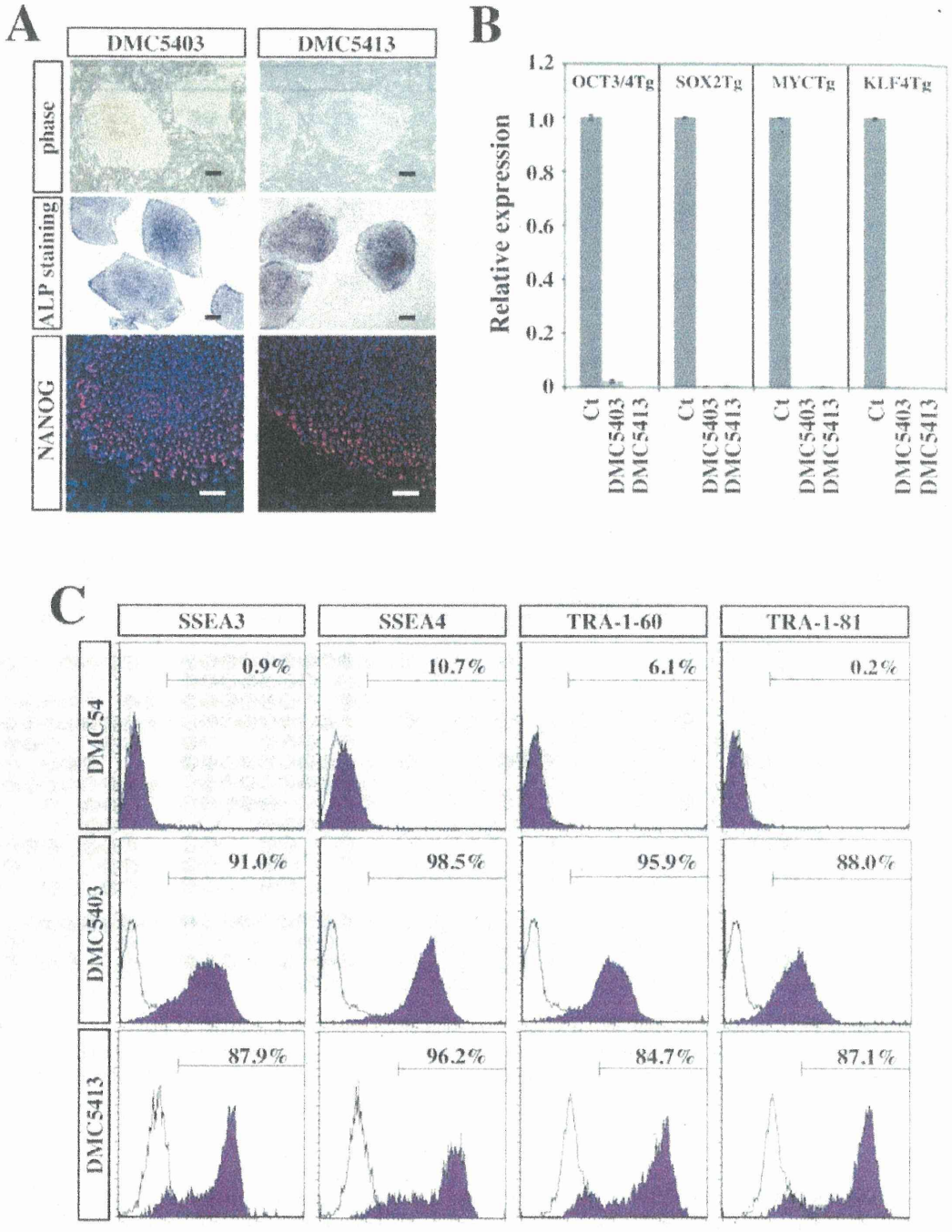

Figure 3. Characterization of decidua-derived mesenchymal cell-derived human induced pluripotent stem cells (DMC-hiPSCs). (A) Representative results of morphology and cytochemical analyses. Morphology (top), ALP staining (middle), and Nanog protein staining (bottom) of DMC-hiPSCs. Scale bar: 200 μm (morphology and ALP staining) and 50 μm (Nanog staining). (B) Expression of the four exogenous transgenes (OSKM) in DMC-hiPSC clones (DMC5403 and DMC5413) relative to infected cells extracted on day 3 postinfection (mean±SD, 3 independent experiments). (C) Flow cytometry analysis of hESC-specific cell surface markers [stage-specific embryonic antigen 3 (SSEA3), SSEA4, TRA-1-60, and TRA-1-81]. The shaded histograms represent the distribution of cells stained by the respective antibodies, and the open histograms show the isotype control staining.

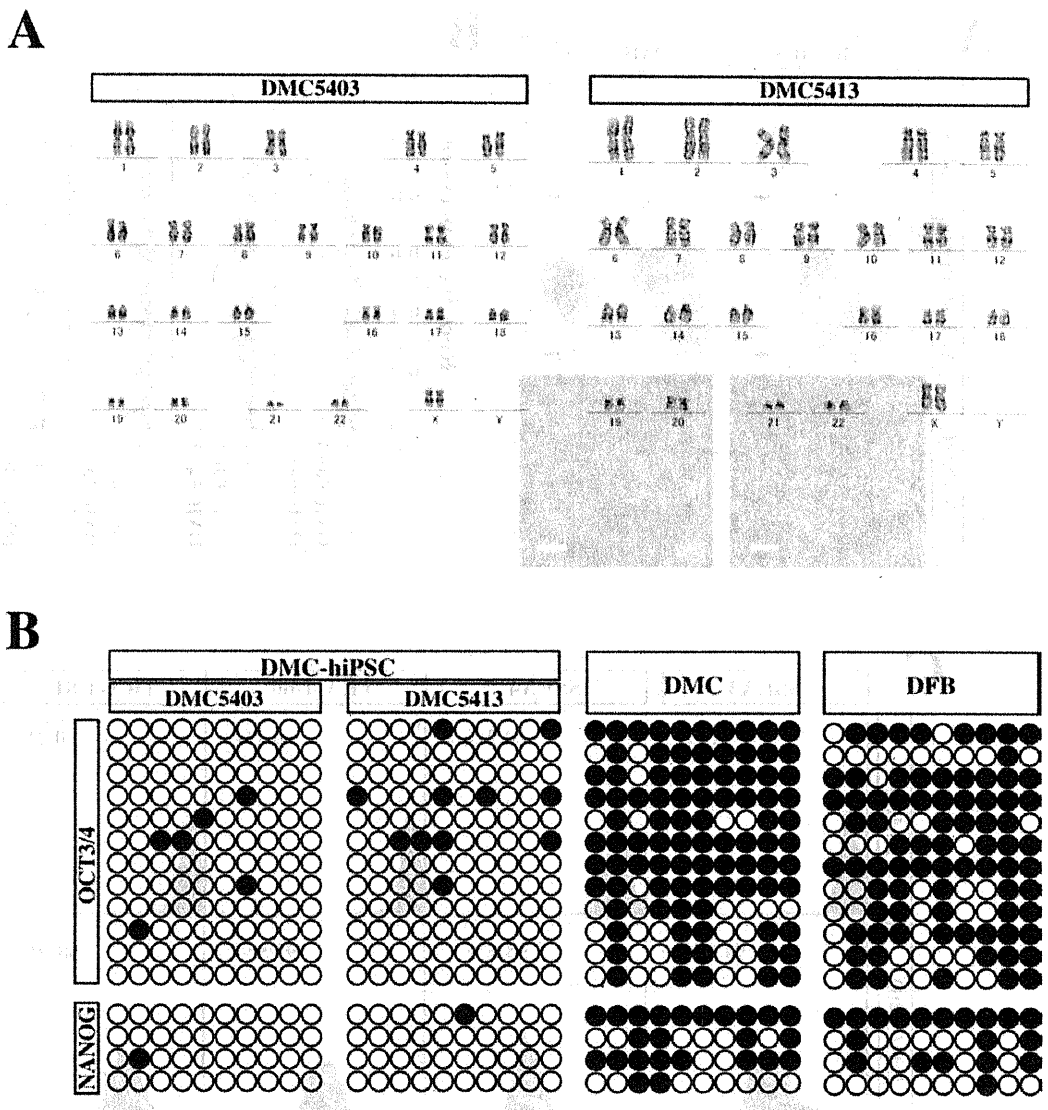

Figure 4. Genomic DNA analysis of DMC-hiPSCs. (A) Representative G-banding karyotype analysis of DMC-hiPSCs (DMC5403 and DMC5413). The DMC-hiPSC clones showed a normal karyotype at passage 30 and 38, respectively. (B) DNA methylation profile of the OCT3/4 and NANOG promoters in the DMC-hiPSCs, parental DMCs, and DFBs. ○Unmethylated CpGs; ●methylated CpGs.

(Fig. 5A), and qRT-PCR analysis showed the down-regulated expression of pluripotent stem cell marker genes [hESCs: OCT3/4, NANOG, and telomerase reverse transcriptase (TERT)] (Fig. 5B). The expression of differentiation-specific marker genes of the three germ layers [endoderm: forkhead box A2 (FOXA2), SOX17, AFP, and albumin (ALB); mesoderm: GATA binding protein 4 (GATA4), Brachyury, Mut S homolog (msh) homeobox 1 (MSX1), and NK2 transcription factor related, locus 5 (NKX2-5); ectoderm: neurogenin 2 (NEUROG2), SOX1, and paired box 6 (PAX6); epidermis: keratin 17 (KRT17)] was observed in these EBs (Fig. 5B). The expression levels of the differentiation-specific marker genes were equal to or surpassed those in EBs formed from 201B7 hiPSCs (Fig. 5B).

To confirm the progression of differentiation, we replated the 10-day-cultured EBs on gelatin-coated chamber slides, cultured them in 10% FBS-containing medium for an additional 2 weeks, and then examined the cells by immunocytochemistry on day 24 of total in vitro differentiation. On day 24, the cells in EBs had differentiated into various adherent cells, most of

Table 2. Short-Tandem Repeat (STR) Genotyping

Locus/Clone	DMC54	DMC5403	DMC5413	UCB54
Penta_E	18, 21	18, 21	18, 21	14, 18
D18S51	14, 16	14, 16	14, 16	14, 15
D21S11	31.2, 33.2	31.2, 33.2	31.2, 33.2	31.2, 33.2
TH01	9, 9	9, 9	9, 9	7, 9
D3S1358	15, 16	15, 16	15, 16	14, 15
FGA	19, 22	19, 22	19, 22	19, 23
TPOX	8, 9	8, 9	8, 9	8, 11
D8S1179	16, 16	16, 16	16, 16	10, 16
vWA	14, 16	14, 16	14, 16	16, 16
Amelogenin	X, X	X, X	X, X	X, Y
Penta_D	11, 15	11, 15	11, 15	11, 12
CSF1PO	11, 12	11, 12	11, 12	11, 11
D16S539	9, 12	9, 12	9, 12	9, 9
D7S820	8, 11	8, 11	8, 11	11, 12
D13S317	8, 8	8, 8	8, 8	8, 11
D5S818	11, 13	11, 13	11, 13	8, 11

Fifteen polymorphic STR DNA loci plus Amelogenin (AMEL) for sex chromosomes were analyzed.

which expressed very little NANOG (Fig. 5C), although some expressed endoderm markers (CK19), mesoderm markers (desmin, αSMA), and ectoderm markers (βIII-tubulin, GFAP) at various levels (Fig. 5C). These results indicated that the DMC-hiPSCs were fully pluripotent in vitro.

In Vivo Differentiation of DMC-hiPSCs

The pluripotency of the DMC-hiPSCs was also evaluated by an in vivo teratoma formation assay. DMC-hiPSCs formed tumor masses in NOG mice after several months, and these tumor masses contained histological components of the three germ layers. Some tumors showed neuroepithelial-like structures that expressed human NCAM (ectoderm) (Fig. 6). The tumors also showed blood vessels and fibrous stroma that were positive for human vimentin, muscle-like structures that expressed desmin (mesoderm), and gut-like epithelium that was positive for epithelial membrane antigen (EMA) or cytokeratin (endoderm) (Fig. 6). Thus, the DMC-hiPSCs formed teratomas showing in vivo pluripotency, which indicated that the DMC-hiPSCs met the criteria for hiPSCs.

Gene Expression Profile of DMC-hiPSCs

To further characterize the DMC-hiPSCs at the molecular level, we examined the genome-wide gene expression profile of two DMC-hiPSCs in comparison to those of hESCs and the parental DMCs. Microarray analysis verified that there was a large difference in the transcriptome profile between the DMC-hiPSCs and parental DMCs and, in contrast, a strong similarity between that of the DMC-hiPSCs and KhES1 (Fig. 7A). Many undifferentiated ES cell marker genes (2), such as OCT3/4 (POU5F1), SOX2, NANOG, TERT, FOXD3, growth differentiation factor 3 (GDF3), zinc finger protein 42 homolog (ZFP42/reduced expression protein 1 [REX-1]), and teratocarcinoma-derived growth factor 1 (TDGF1), were expressed in the DMC-iPSCs at the same level as in the hESCs (Table 3), although these transcripts were not detected in the parental DMCs.

Among the 108 probe sets in the Human Genome U133 plus 2.0 Array for characterizing undifferentiated stem cells (2), the expression of the X (inactive)-specific transcript (nonprotein coding) gene (XIST) in one of the DMC-iPSCs (DMC5403) was more than 10 times that in the hESCs and was the same as in the parental DMCs (Table 3). Quantitative RT-PCR analysis for the XIST gene expression showed that the expansion and continuous passage of DMC-iPSCs led to the loss of XIST transcription in clone DMC5403 (Fig. 7B). The other DMC-iPSC clone (DMC5413) and a female DFB-iPS clone expressed XIST at a very low level at the beginning of culture (less than 10 passages) and after many passages (no less than 27 passages) (Fig. 7B). The methylation status of the XIST promoter region was assessed by methylation-specific PCR. Genomic DNA extracted from the parental female cells and DMC-hiPSC clone 5403 produced similar amounts of PCR products with both methylated and unmethylated DNA-specific primer sets. In contrast, the methylated DNA-specific primer set produced almost all the amplified products from the other clone, 5413, and the female DFB-hiPSCs (Fig. 7C).

Recently, new key molecules for efficient reprogramming, lung carcinoma-derived Myc (MYCL1) and glioma-associated oncogene similar protein [GLIS] family zinc finger (GLIS1), were reported (24,36). We evaluated the expression of these genes and of other GLI-related Krüppel-like zinc finger genes, GLIS2 and GLIS3, in several cell lines and tissues (Fig. 8A). Quantitative RT-PCR analysis showed that MYCL1 was expressed in all the primary cells, with the DFBs expressing three to four times the level observed in the placenta-derived cells or BM-MSCs. GLIS1 expression was detected in the testis at a high level and in the placenta at a moderate level. Of the primary cells, a low level of GLIS1 expression was detected in only the AECs and DMCs; no significant expression of GLIS1 was detected in the hESCs or hiPSCs. On the other hand, significant amounts of GLIS2 and GLIS3 were expressed in the placenta-derived cells, DFBs, and BM-MSCs, while very low levels were expressed in pluripotent stem cells, testis, and placenta (Fig. 8A). Seventeen factors that can substitute for Klf4 have been identified, although they have much lower efficiencies in iPSC generation (24). Among these factors, we evaluated Zinc finger and SCAN domain containing 4 (Zscan4), which is expressed exclusively in mouse late

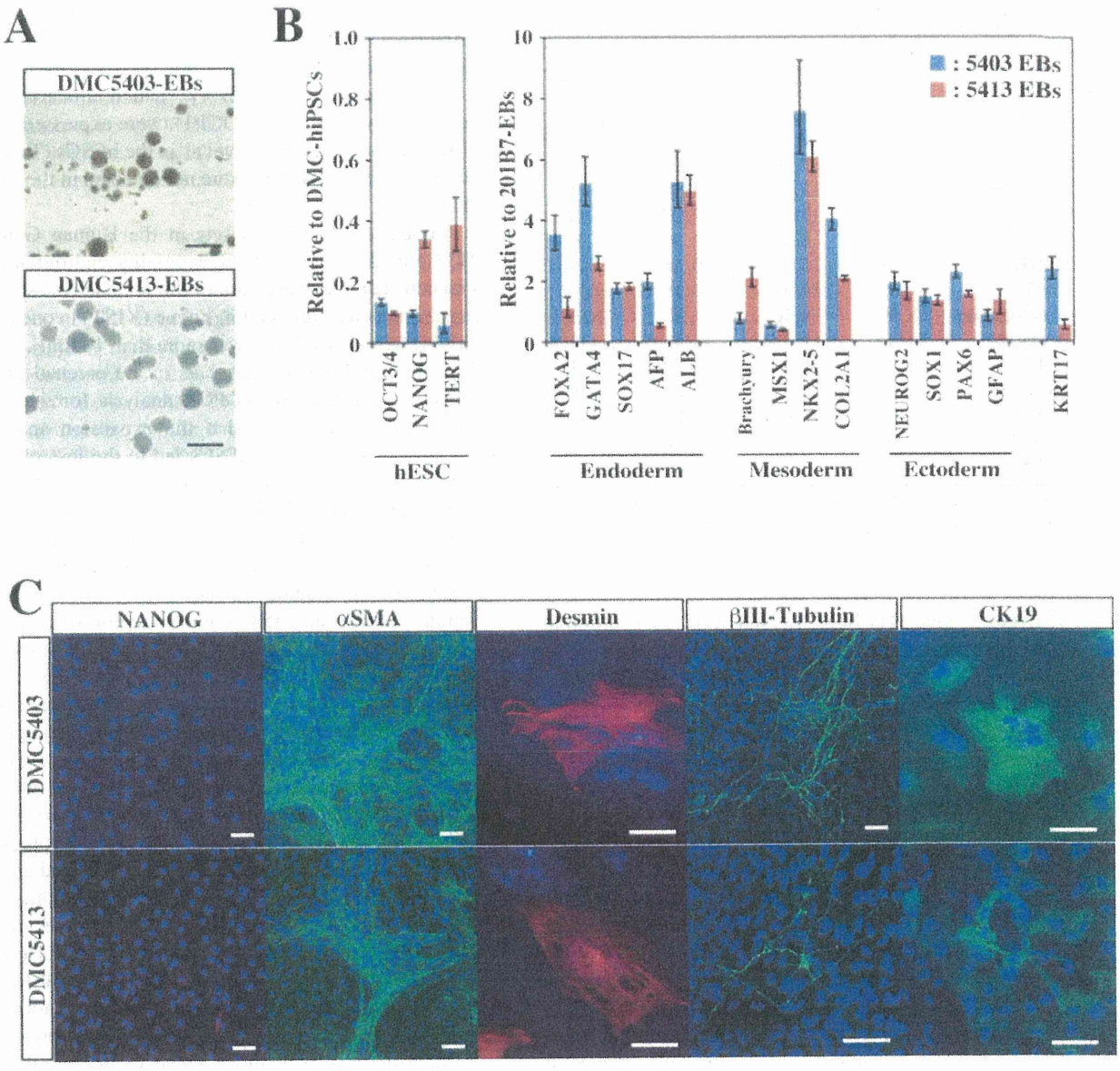

Figure 5. In vitro differentiation of DMC-hiPSCs. (A) Embryoid bodies (EBs) derived from two DMC-hiPSC clones on day 10. Scale bar: 200 μm. (B, left) Expression of human pluripotent stem cell marker genes in the same EBs on day 10 in suspension culture compared with their corresponding DMC-hiPSCs. (Right) Differentiation-specific marker gene expression relative to that of EBs derived from 201B7. (C) Immunofluorescence staining of differentiated cells in Dulbecco's modified Eagle's medium (DMEM) containing 10% fetal bovine serum (FBS) for an additional 2 weeks. Scale bars: 50 μm. See Table 1 for gene definitions.

two-cell embryos and embryonic stem cells (7). ZSCAN4 expression was detected in five primary cultured cells at very low levels, but was roughly five times higher in AECs and DFBs than in AMCs, DMCs, or BM-MSCs (Fig. 8A). We also examined the expression of GLIS1 and ZSCAN4 in DFBs and DMCs 3 days after the transduction of OSKM. Under this condition, we observed an increase in ZSCAN4 but not in GLIS1 expression in both DFBs and DMCs (Fig. 8B).

DISCUSSION

DMCs Are a Promising Human Allogeneic Cell Type for Generating hiPSCs

In this study, we demonstrated that hiPSCs were efficiently generated from DMCs, which were derived from the maternal components of placental tissue. The DMC-hiPSCs maintained a normal karyotype and showed equivalent characteristics to hESCs in colony morphology, global gene expression profile (including human